THE JOURNAL OF PHYSICAL CHEMISTRY B
A JOURNAL OF THE AMERICAN CHEMICAL SOCIETY

pubs.acs.org/JPCB

Article

Exploration of Gas–Liquid Interfaces for Liquid Water and Methanol Using Extreme Ultraviolet Laser Photoemission Spectroscopy

Yo-ichi Yamamoto, Tatsuya Ishiyama, Akihiro Morita, and Toshinori Suzuki*

Cite This: *J. Phys. Chem. B* 2021, 125, 10514–10526

Read Online

ACCESS | Metrics & More | Article Recommendations | Supporting Information

ABSTRACT: We present a study using extreme UV (EUV) photoemission spectroscopy of the valence electronic structures of aqueous and methanol solutions using a 10 kHz EUV light source based on high-order harmonic generation and a magnetic bottle time-of-flight electron spectrometer. Two aspects of the observed spectra are highlighted in this study. One is variation of the vertical ionization energy (VIE) for liquids as a function of the solute concentration, which is closely related to surface dipoles at the gas–liquid interface. The experimental results show that the VIE of liquid water increases slightly with increasing concentrations of NaCl and NaI and decreases with NaOH. The VIE of liquid methanol was also found to change slightly with NaI. On the other hand, tetrabutylammonium iodide (TBAI) and butylamine (BA) clearly reduce the VIE for liquid water, which is attributed to the formation of an electric double layer (EDL) by segregated solutes at the gas–liquid interface. As evidence for this, when the pH of an aqueous BA solution is reduced to protonate BA, the VIE shift gradually decreases because the protonated BA moves into the bulk to suppress the influence of the EDL. We computed the surface potentials for these solutions using molecular dynamics simulations, and the results supported our interpretation of the experimental results. Another observation is the variation of the relative energy and shape of individual photoelectron bands for solvents, which is related to alteration of the structure and constituents of the first solvation shell of ionized solvent molecules. All of the solutes cause changes in the photoelectron spectra at high concentration, one of the most prominent of which is the degree of splitting of the $3a_1$ band for liquid water and the $7a'$ band for liquid methanol, which are sensitive to hydrogen bonding in the liquids. The $3a_1$ splitting decreases with the increasing concentration of NaI, NaCl, and NaOH, indicating that Na^+ penetrates into the hydrogen-bonding network to coordinate to a nonbonding electron of a water molecule. On the other hand, TBAI and BA cause smaller changes in the $3a_1$ splitting. Full interpretation of these spectroscopic features awaits extensive quantum chemical calculations and is beyond the scope of this study. However, these results illustrate the strong potential of EUV laser photoemission spectroscopy of liquids for exploration of interfacial and solution chemistry.

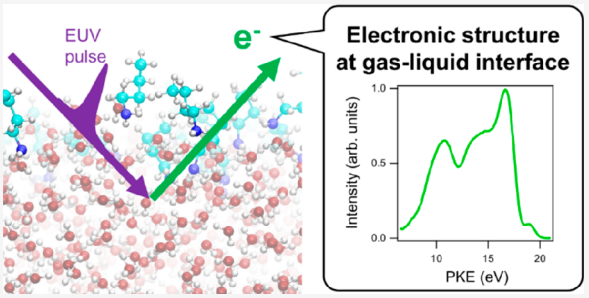

INTRODUCTION

The influences of solute on the hydrogen bonding and electronic structure of liquid water have been attracting much interest over the years.[1−7] In this study, we explore this problem from the viewpoint of the electron binding energy (eBE) measured using extreme UV (EUV) photoemission spectroscopy. Photoemission spectroscopy using a liquid microjet technique was pioneered by Faubel and colleagues,[8,9] and considerable progress has been made since then.[10−13] The vertical ionization energies (VIE) for liquid water, methanol, and ethanol were initially reported to be 10.92, 9.99, and 9.66 eV,[8] and these values have since been refined to 11.31(4),[14] 9.70(7), and 9.52(7) eV,[15] respectively. Rigorously speaking, however, none of the aforementioned values are for a pure solvent. Because liquid microjets are inevitably charged by an electrokinetic charging effect,[16] a small amount of electrolyte is always added into these solvents to mitigate this effect.[14,17] Furthermore, as will be described later, all energy calibration methods for liquid photoemission spectra require the addition of electrolytes. In our most recent He(II) photoemission spectroscopy study of methanol and ethanol,[15] the concentration of the electrolyte was only 1 mM, yet its addition was indispensable for accurate measurements. Because the VIE for a solvent is unaltered by addition of a small amount of solute, these measurements provide accurate estimates of the VIE for pure solvents. On the other hand, at high solute concentrations, the electronic structure of a solvent will be influenced by the solute.[18,19] Moreover, if a solute is segregated at the gas–liquid interface, the local solute density becomes considerably higher than the bulk value.[20−23] Therefore, even

Received: May 30, 2021
Revised: August 26, 2021
Published: September 8, 2021

a low bulk concentration can cause a large impact on the properties at the gas−liquid interface probed by photoemission spectroscopy. The magnitude and specificity of such influences are of interest.

Before we discuss the photoemission spectra of aqueous and methanol solutions, we would like to clarify the nomenclature used in our discussion. We refer to the molecular orbitals relevant to photoemission spectra using the orbital names for water vapor and methanol molecules. This conventional nomenclature is practical in that the energetic ordering of molecular orbitals is unchanged upon condensation. However, it should be kept in mind that this is not rigorous from the viewpoint of group theory, as the system is no longer represented by a point group. For example, the splitting of the $3a_1$ (HOMO−1) orbital of liquid water will be discussed later, even though a_1 is the notation used for a nondegenerate orbital in an isolated water molecule; the splitting is due to donor−acceptor interactions caused by hydrogen bonding and conjugation of molecular orbitals.[24] We refer to the general kinetic energy distribution of electrons emitted by light irradiation as the *photoemission* spectrum. The term *photoelectron* spectrum is specifically used to describe the distribution of primary electrons emitted by the photoelectric effect. All spectra discussed in this paper are of the photoelectrons, except for a low-energy background signal.

An early study by Weber et al. using soft X-ray photoemission spectroscopy indicated that the photoemission spectra of aqueous alkali metal halide (NaX) solutions are unchanged up to rather high concentrations (12 M for NaI).[25] This notion, however, was questioned by Olivieri et al., who showed that the O(1s) ionization energy for liquid water varies with the concentration of butylamine (BA).[23] Pohl et al. have revisited the photoemission spectra of aqueous NaI solution for concentrations up to 8 M, and they showed that the $1b_2$ and $3a_1$ band positions relative to the $1b_1$ band vary only slightly with electrolyte concentration;[18] however, they did not address the concentration dependence of the absolute ionization energy for liquid water because of the technical difficulties described below. Thus, the claim by Olivieri et al. has not been fully addressed.

Photoemission spectroscopy requires careful calibration of the absolute kinetic energy of electrons. Calibration has most often been performed by using gaseous samples for which ionization energies are precisely known. The gas calibration method employs adjustment of the electrolyte concentration of a solution, as discussed by Kurahashi et al., to equalize the vacuum levels between the ionization points for a liquid and a reference gas.[14] Because of this strict requirement, it was not possible to perform precise measurements of the VIE for arbitrary electrolyte concentrations. A similar calibration method using a reference gas proposed by Olivieri et al. was to apply a small bias voltage to a liquid microjet to adjust the vacuum levels between the ionization positions for a liquid and a gas,[23] which in principle enables measurements at any arbitrary concentration. However, the results so far obtained with this method have not been fully verified, and further examination seems necessary. The third method is to use the low-energy cutoff of a photoemission spectrum of a liquid as the reference energy,[19,23,26] which has previously been employed in photoemission spectroscopy of solid samples.[27] An essential difference between this method and the first two methods is that the cutoff energy corresponds to the local vacuum level just outside the liquid rather than the vacuum level at a position distant from the liquid. This third method requires applying a bias voltage (<−10 V) to a liquid microjet to upshift the entire electron kinetic energy (eKE) distribution because electrons with energies close to 0 eV are never detected without a bias voltage. The bias voltage also ensures that the work function of the analyzer does not dictate the cutoff energy. The energy difference between the cutoff energy and the measured eKE provides the absolute eKE with reference to the local vacuum level. Thus, the third method enables measurement of photoemission spectra of liquids for arbitrary solute concentrations without using gaseous reference samples. Very recently, Thürmer et al. presented a detailed discussion on these calibration methods and indicated that the VIE for a liquid is invariant with NaI addition, but it decreases with tetrabutylammonium iodide (TBAI) addition.[19]

An important question regarding photoemission spectroscopy of liquids is its probing depth. As reviewed in the literature,[11,28] the probing depth for photoemission spectroscopy of liquids has not been established for an electron kinetic energy lower than 100 eV, even for the most fundamental liquid of water. This is due to the lack of precise estimation of the electron scattering cross sections in liquids either theoretically or experimentally in this energy region.[11,29] However, the probing depth in this study is crudely estimated to be on the order of a nanometer; therefore, our EUV photoemission spectroscopy results are sensitive to, albeit not exclusively, the gas−liquid interface. When solutes are segregated at the surface, the photoemission signal is produced unambiguously from several molecular layers near the liquid surface. For example, we have previously performed time- and angle-resolved photoelectron spectroscopy (TARPES) of charge transfer to solvent (CTTS) reactions from 1,3-diazabicyclo[2.2.2]octane (DABCO) or TBAI to liquid water. Clear photoelectron angular anisotropy was observed for DABCO solution, indicating that the photoelectron signals are from molecules segregated at the gas−liquid interface.[21] On the other hand, photoelectrons from an aqueous TBAI solution exhibited much weaker anisotropy, indicating that I^- resides at a larger depth than DABCO.[21]

The electronic structure and dynamics at the gas−liquid interface have been investigated extensively by using nonlinear optical spectroscopy approaches such as second harmonic generation (SHG) and sum-frequency generation (SFG).[30−33] In these methods, surface-selective observations were ensured by focusing on the second-order nonlinear susceptibility that becomes nonzero in the spatial region where inversion symmetry is broken. On the other hand, when a strong local electric field is present at the gas−liquid interface, for example by adsorption of charged amphiphilic compounds, the inversion symmetry is broken for a depth greater than a single molecular layer. Then, the third-order nonlinear response involving the local electric field creates SHG and SFG signals not only from the top molecular layer at the gas−liquid interface but a deeper spatial region.[34] Under these circumstances, the probing depths of nonlinear spectroscopy and EUV photoemission spectroscopy are expected to be similar, allowing complementary information to be obtained on the structure and dynamics of the interfacial region.

In this study, we investigate the variation of the electronic structure of liquid water and methanol using EUV photoemission spectroscopy. Liquid water is of paramount importance in chemical, biological, and environmental sciences, and it is the central target of our study. Methanol

https://doi.org/10.1021/acs.jpcb.1c04765
J. Phys. Chem. B 2021, 125, 10514−10526

is a variant of water created by replacing a hydrogen atom with a methyl group; while liquid water has a tetrahedral hydrogen-bonding network provided by a double proton donor and double proton acceptor structure, methanol has a one-dimensional chain structure of hydrogen bonds with a single donor and single acceptor configuration. Unlike our previous studies on these solvents using a hemispherical electron energy analyzer (HEA) and (quasi-)continuous radiation from a synchrotron radiation facility[24] or a He discharge lamp,[15] we employ a magnetic bottle time-of-flight (MBTOF) electron energy analyzer[35] and a table-top EUV laser based on high-order harmonic generation (HHG),[36−39] which are the standard instruments in time-resolved photoemission spectroscopy (TRPES). HEA is superior to a MBTOF analyzer in terms of energy resolution, especially at high electron kinetic energies in the X-ray region. On the other hand, a MBTOF analyzer offers an extremely high electron collection efficiency of over 50% and the capability of measuring the entire photoemission spectrum on a shot-to-shot basis (the TOF method requires a pulsed light source). These features make a MBTOF spectrometer an ideal instrument for TRPES; moreover, the combination of a MBTOF analyzer and a 10 kHz pulsed laser provides an extremely high data acquisition rate. Our experimental results reveal that some solutes cause an energy shift of the entire photoemission spectrum of a solution and that all solutes induce some spectral changes at high concentrations. To study the spectral energy shift, we compare the experimental results with those for the liquid surface potential computed by using classical molecular dynamics simulations.[40−43] To our knowledge, such a comparison has not been attempted previously.

EXPERIMENTAL METHODS

All measurements were performed by using a MBTOF spectrometer[44] and a table-top EUV laser.[45] We have determined the photon energy accurately to be 27.5 eV using photoemission spectroscopy of Xe and nitric oxide. This photon energy is of the ninth harmonic of the 400 nm driving laser and is a typical probe photon energy in our EUV-TRPES studies of aqueous solutions. We applied a negative bias voltage of −10.0 V to a liquid microjet to shift the entire eKE distribution into the region where a uniform transmission efficiency through the spectrometer is ensured. We measured the photoemission spectrum and determined the true eKE by taking the difference between the measured kinetic energy and the cutoff energy. The cutoff energy was determined by using the inflection point found by taking the second derivative of the photoemission spectrum in the cutoff region (see the Supporting Information for more details). However, the spectrum thus measured contained signals from gaseous species. Therefore, we also measured a spectrum by applying a lower bias voltage, typically −35.0 V, to the liquid microjet to remove the signals from the gaseous species.[15,19,46,47] This provides a greater energy shift in the photoemission spectrum of a liquid, while photoelectrons from a gas undergo much less acceleration because the electric potential outside the liquid rapidly converges to 0 V at the entrance skimmer for the MBTOF spectrometer. We applied a retarding potential of −25.0 V to the flight tube inside of MBTOF to decelerate the incoming electrons and enhance the kinetic energy resolution. The drawback of the latter method is a slightly lower accuracy in determining the cutoff energy. Thus, we combined these two methods (−10.0 V or −35.0/−25.0 V) to analyze the liquid photoemission spectrum. The energy resolution of the electron energy analyzer and the overall energy resolution including the EUV radiation bandwidth are estimated to be 0.05 and 0.1 eV, respectively, based on the photoelectron spectra of gaseous samples. The photoemission spectrum of a liquid consists of a well-resolved valence band structure and a broad background that increases in intensity toward zero eKE.[48] This background signal is due to inelastically scattered photoelectrons, low-energy photoelectrons produced by intermolecular Coulombic decay,[49] and secondary electrons from electron impact ionization induced by photoelectrons traveling in the liquid. The spectral shape of the background can be well expressed by using a Gaussian function. Thus, we analyzed each spectrum by using least-squares fitting based on the valence bands and the broad background. A typical fit is shown in Figure 1. The spectra presented later are those after

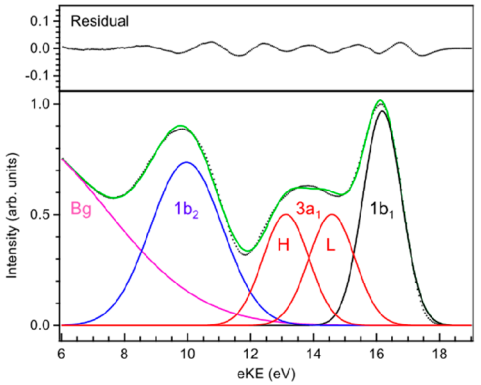

Figure 1. Photoemission spectrum of 50 mM aqueous NaCl solution and least-squares fitting results. The notations $1b_1$, $3a_1$, and $1b_2$ indicate the electron orbitals for water molecules with a C_{2v} point group. Bg indicates the background photoemission signal.

subtraction of the broad background. The analysis of the $1b_2$ band is inevitably less accurate because of the overlap with the broad background signal and the influence of inelastic scattering effects. Here we present the positions of $1b_2$ bands but exclude them from our detailed discussion. We will focus on the concentration dependence of the $1b_1$ band, which is often used as an internal energy standard in photoemission spectroscopy of aqueous solutions, and on the variation in the $3a_1$ band, which is sensitive to the hydrogen-bonding structure of liquid water.

A 10 kHz one-box Ti−sapphire regenerative amplifier (35 fs, 800 nm (ω)) was used to produce EUV pulses. The fundamental output of the amplifier was converted to 2ω laser pulses in a 0.3 mm thick β-barium borate (BBO) crystal and focused into a Kr gas cell by using a quartz lens (f = 500 mm) to induce HHG. A single-order harmonic was isolated by using a time-preserving monochromator.[50] The full width at half-maximum (FWHM) of the EUV beam at the microjet was about 100 μm. A continuous liquid microjet was introduced into a photoionization chamber through a 25 μm i.d. graphite-coated fused silica capillary at a flow rate of 0.5 mL/min. The capillary was connected to a stainless steel nozzle assembly, and a bias voltage was applied to the entire nozzle assembly. The microjet discharged from the nozzle generally underwent disintegration within a traveling distance of 10 mm owing to amplification of microscopic turbulence. The disintegrated liquid droplets were collected with a liquid-nitrogen-cooled

https://doi.org/10.1021/acs.jpcb.1c04765
J. Phys. Chem. B 2021, 125, 10514−10526

trap. A SmCo permanent magnet with a soft iron cone was placed 2 mm away from the liquid microjet in the photoionization chamber to provide a strong magnetic field of about 1 T. A weak magnetic field (1 mT) was applied to the flight tube along its flight axis by using a solenoid coil (300 turns/m, 3 A). The combination of the strong and weak magnetic fields provided a magnetic bottle effect to collect more than 50% of the photoelectrons emitted from the liquid. The entire photoionization chamber and the energy analyzer were magnetically shielded against the terrestrial magnetic field with a permalloy inner layer placed inside the vacuum. A variable retardation potential was applied to the flight tube to decelerate photoelectrons, and the electrons were detected by using a Chevron microchannel plate (MCP) with a 38 mm effective diameter and a preamplifier, and electron counts were integrated by using an analog-to-digital converter. The electron flight length was 1.2 m. A more detailed description of the MBTOF spectrometer can be found in a previous paper.[44]

COMPUTATIONAL METHOD

We performed molecular dynamics simulations on aqueous solutions using the SPC/E model[7] for water. We employed the general AMBER force field[51] for TBA^+, BA, and BAH^+ (protonated BA) with partial charges determined by a restrained electrostatic potential fit[52] to the potential calculated at the B3LYP/6-31G(d, p) level of theory and the force field model for ions compatible with the SPC/E model (the partial charges employed for simulations are listed in the Supporting Information).[53] Initial configurations were prepared in the following way. A rectangular simulation box was prepared with a slab geometry. The box dimensions $L_x \times L_y \times L_z$ were $40 \times 40 \times 250$ Å^3 for a system with 3000 water molecules and $40 \times 40 \times 370$ Å^3 for that of 6000 water molecules, and the interface was set parallel to the x–y plane. Initially, water and solute molecules were placed at random positions and with random orientations in the middle of the simulation cell (see Figure 2)

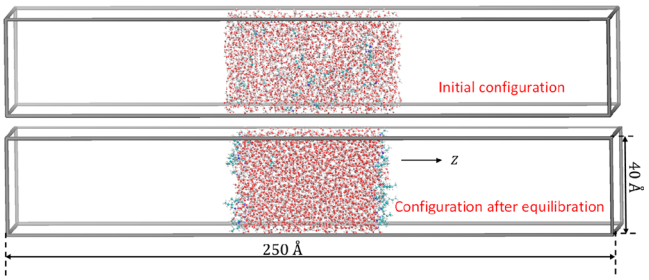

Figure 2. Snapshots of initial configuration (top) and configuration after equilibration (bottom) of aqueous TBAI solution containing 3000 water molecules and 50 solute molecules (ion pairs).

by using the PACKMOL package.[54] The steepest descent method was used to remove initial overlaps of molecules. Newton's equation of motion was solved by using the leapfrog algorithm,[55] with a time step Δt = 2.0 fs with three-dimensional periodic boundary conditions, where the bonds with H were treated by using a linear constraint solver.[56] In the equilibration step, a constant number, volume, and temperature (NVT) ensemble simulation was carried out, where the system temperature was kept at T = 298.15 K by using a Nosé–Hoover thermostat.[57,58] The long-range Coulombic interactions were treated by using the particle-mesh Ewald method.[59,60] The cutoff length of the Lennard-Jones potential and the real-space part of the Ewald sum were taken to be 10 Å. A simulation for at least the time period of 60 ns was necessary to reach an equilibrium state. The subsequent 10 ns production run was conducted with 32 parallel computation starting from different initial configurations; hence, a total ensemble average was taken for 320 ns. The GROMACS package (ver. 5.1.2)[61] was employed for these trajectory calculations.

The surface potential (χ) is defined as the difference in the electric potential ϕ given by the following formula:

$$\chi = \phi(z_1) - \phi(z_0) = -\int_{z_0}^{z_1} \mathrm{d}z'\, E_z(z') \tag{1}$$

$$E_z(z) = \frac{1}{\varepsilon_0}\int_{z_0}^{z} \mathrm{d}z'\, \rho_q(z') \tag{2}$$

where z_0 and z_1 represent arbitrary positions in the vacuum and the liquid, respectively, so that the integral of eq 1 encompasses the interfacial region. $\rho_q(z)$ and $E_z(z)$ are the charge density and the normal component of the electric field at z, respectively, and ε_0 is the permittivity of free space. The absolute value of χ depends on the computational method and the molecular potential; for example, an estimation based on ab initio calculations predicts χ for liquid water to be +3.1 V, while a classical simulation based on atomic partial point charges yields about −0.5 V.[62] However, in this study, we focused on the relative shift of χ from the value for pure water by addition of solutes, which is free from any ambiguity in the absolute value of χ. The orientation distribution for water molecules is defined as $\rho\langle\cos\theta\rangle$, where ρ is the number density for water molecules and $\langle\cos\theta\rangle$ is the average direction cosine (θ is the angle between the OH bond and the surface normal unit vector). When this value is negative, the OH bond is pointing toward the bulk on average.

RESULTS

Aqueous NaX Solutions (X = Cl, I, and OH). Figure 3 shows the photoelectron spectra of aqueous solutions of (a) NaCl, (b) NaI, and (c) NaOH at various concentrations. The signal intensity in each spectrum is normalized by the $1b_1$ (HOMO) band for liquid water. The axes at the bottom and top indicate the photoelectron kinetic energy (PKE) and the eBE, the latter being the difference between the photon energy and the PKE. These strong electrolytes completely dissociate and dissolve in an aqueous solution, and in the case of NaI, iodine is known to have a higher surface density compared to the bulk value.[6] In all cases, the position of the $1b_1$ band in the photoelectron spectrum changed only slightly with concentration. The relative band positions observed for aqueous NaI solutions agree with Pohl et al.[18] The intensities of the $3a_1$ and $1b_2$ bands increase and the $3a_1$ bandwidth clearly decreases with increasing the NaI concentration. The band associated with I^- is well separated from those for liquid water, indicating clear spin–orbit splitting (5p $^2P_{3/2}$ and $^2P_{1/2}$). The photoelectron spectra of aqueous NaOH solution, shown in Figure 3c, exhibit a similar concentration dependence, except that the variation in the intensity of the $1b_2$ band is smaller than that for aqueous NaCl and NaI solutions, and the OH^- band is weaker than the Cl^- and I^- bands for a given concentration. It should be noted that the effect of NaOH is slightly different from that of NaCl and NaI in that it changes the pH of the solution; for example, addition of 1 M NaOH changes the pH from 7 to 14.

https://doi.org/10.1021/acs.jpcb.1c04765
J. Phys. Chem. B 2021, 125, 10514–10526

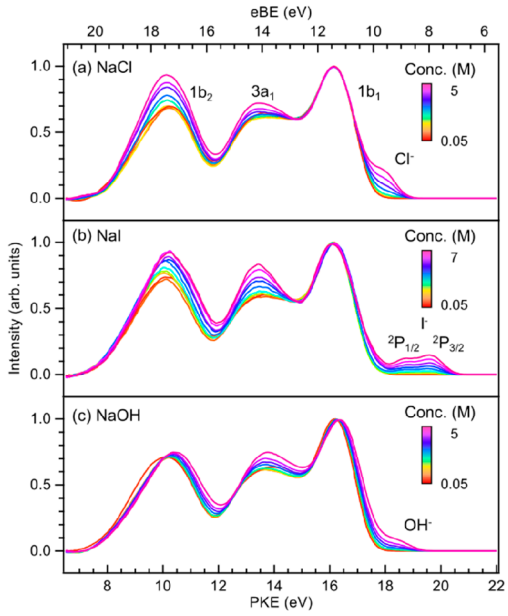

Figure 3. Photoelectron spectra showing valence bands for aqueous solutions of (a) NaCl, (b) NaI, and (c) NaOH at various concentrations. The signal intensity of each spectrum is normalized to the $1b_1$ (HOMO) band of liquid water.

We performed least-squares fitting of these spectra by assuming Gaussian functions for each band; the representative fits are seen in Figure 1. As described in the Introduction, the $3a_1$ band for liquid water consists of two components ($3a_1$H and $3a_1$L), which are split as a result of hydrogen bonding.[24] In the fitting process, we assumed that the $3a_1$H and $3a_1$L bands have the same Gaussian shape and intensity (Figure 1). The uncertainties in the band positions estimated by using the least-squares fitting were typically tens of meV, which were much smaller than the spectral resolution (0.1 eV). Figure 4 summarizes the estimated shifts of photoelectron bands

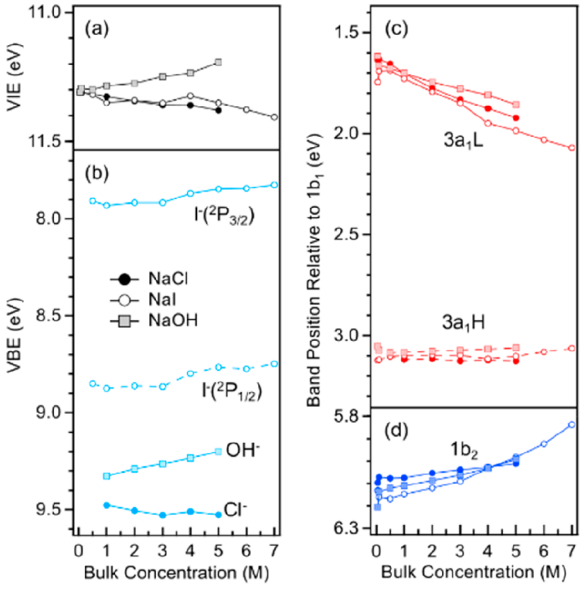

Figure 4. Photoelectron band positions for (a) $1b_1$, (b) anions, (c) $3a_1$, and (d) $1b_2$ at various solute concentrations. VIE: vertical ionization energy; VBE: vertical electron binding energy. The experimental uncertainty is ±0.05 eV.

determined in this analysis. The VIE for liquid water, shown in Figure 4a, shows only a slight dependence on the concentration of electrolytes. With increasing concentration, NaOH causes a slight reduction in VIE, while NaCl and NaI cause a slight increase, although the changes are comparable to the experimental energy resolution. The results confirm that the VIE of liquid water (11.3 eV) is the most convenient internal energy standard for photoemission spectroscopy of aqueous solutions at low concentrations (<1 M). The precise determination of the positions of solute bands is rather difficult due to their small intensities and spectral overlap with the intense $1b_1$ band; however, our results suggest that they shift only slightly with the concentration.[63]

The relative energies for the $3a_1$ and $1b_2$ bands with respect to the $1b_1$ band are summarized in Figures 4c and 4d, respectively. In the $3a_1$H orbital, there is an in-phase interaction between the $3a_1$ orbital of the ionized molecule and the nonbonding orbitals ($3a_1$ and $1b_1$) of proton acceptor molecules in the first hydration shell. In the $3a_1$L orbital, there is an out-of-phase interaction with the orbitals of the proton acceptors; therefore it is less stable. The experimental results indicate that VBE of $3a_1$H is almost invariant with the concentration, while $3a_1$L gradually shifts to higher eBE (more energetically stabilized). Consequently, the degree of $3a_1$ band splitting decreases with increasing solute concentration in all cases. Figure 5 shows the dependence of the FWHM of the

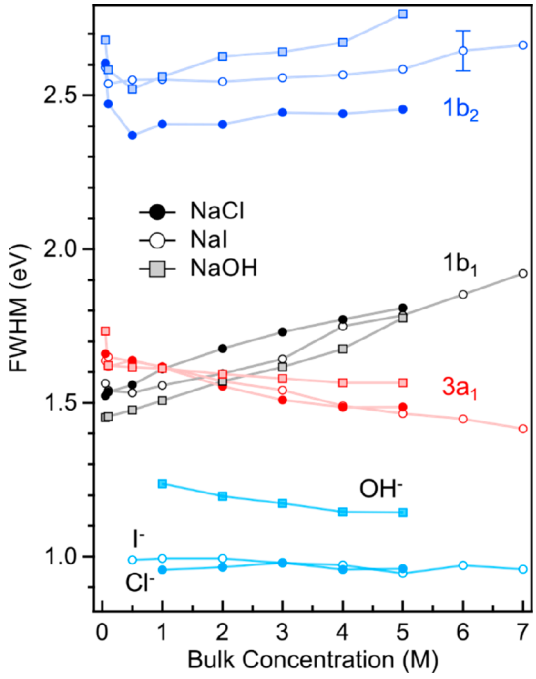

Figure 5. Solute concentration dependence of FWHM for $1b_1$, anions, $3a_1$, and $1b_2$ bands. The FWHM values estimated for the $1b_2$ band were all ±0.065 eV, but for clarity the error bar is only shown for the 6 M case.

photoelectron bands on the solute concentration. The $1b_1$ band exhibits an increase in FWHM with increasing concentration for all electrolytes. The $3a_1$ band exhibits a decrease in FWHM. We examined the validity of the FWHM estimated for the $1b_1$ and $3a_1$ bands by evaluating their integrated intensities (areas). We found that the $3a_1/1b_1$ ratio diminishes to 83% at 7M compared to low concentration

https://doi.org/10.1021/acs.jpcb.1c04765
J. Phys. Chem. B 2021, 125, 10514−10526

owing to the continuous growth of the $1b_1$ bandwidth; the intensity of the $3a_1$ band remained almost constant. Thus, it is likely that the growth of the FWHM of $1b_1$ is overestimated in our results.

Figure 6 shows the dependence of the photoelectron band intensity (integrated area estimated by the curve fitting) for

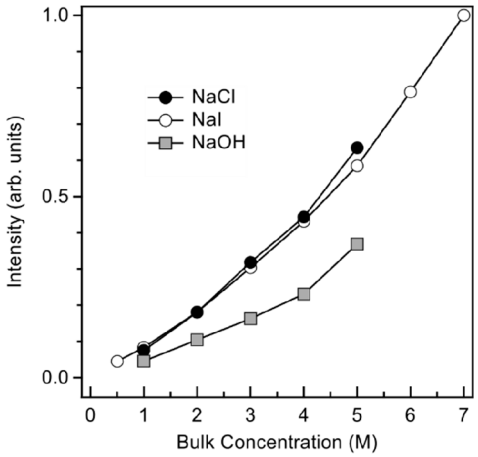

Figure 6. Solute concentration dependence of photoelectron intensity for Cl^-, I^-, and OH^- ions. The intensities are normalized to that of I^- at 7 M.

anions on the solute concentration; as mentioned earlier, these band intensities were normalized by the $1b_1$ (HOMO) band for liquid water. The OH^- band intensity is clearly weaker than those of I^- and Cl^-. The weakness may be partly due to the lower surface activity of OH^- than that of Cl^- and I^-; however, a smaller photodetachment cross section for OH^- is another likely cause. Although the photodetachment cross sections for these anions are unknown in aqueous solutions, they may be crudely estimated from the values in the gas phase[64−66] and those for isoelectronic rare gas atoms.[67] The cross sections thus estimated for I^-, Cl^-, and OH^- are 70, 30, and 10 Mb for a PKE of 10 eV, respectively. Therefore, it is possible that the weaker photoelectron signal associated with OH^- ions is due to the smaller photodetachment cross section. The difference in photoelectron angular anisotropy plays a negligible role in the above discussion, as we employed a MBTOF spectrometer.

Ishiyama and Morita performed molecular dynamics simulations of the gas−liquid interface for aqueous NaI and NaCl solutions using a flexible polarizable water model.[43] Their calculations indicated that the surface potential for these solutions is about −0.4 V, which is almost the same as the value for pure water (−0.421 V). The results of EUV photoemission spectroscopy presented here are consistent with their calculations. Close examination of the experimental results, however, suggests that NaI and NaCl induce a small upshift of VIE of liquid water while NaOH provides an opposite trend, although these shifts are detectable only at high concentrations. These tendencies are consistent with surface enrichment of I^- and Cl^- and a small depletion of OH^- density with respect to Na^+;[68] thus, the directions of surface dipoles due to an electric double layer (EDL) are different between I^-/Cl^- and OH^-. As presented later, the observed effect of NaI is also opposite from that of TBAI which creates an opposite direction of the surface dipole. The results show that the photoemission spectroscopy of liquids is sensitive enough to detect EDLs at the gas−liquid interface, and a comparison of the experimental results with molecular dynamics simulations provides useful insights for understanding interfacial chemistry.

Aqueous Solution of Butylamine (BA). As described in the Introduction, Olivieri et al. investigated the soft X-ray O(1s) photoelectron spectrum of an aqueous 0.05 M NaCl solution with a small bias voltage (a few volts) applied to a microjet.[23] The purpose of the bias voltage was to compensate for any influence of the potential difference around the microjet. When the vacuum level around the jet becomes flat, the O(1s) photoelectron band for water vapor can be used for energy calibration of the photoemission spectrum of liquid water. Using this procedure, they found that the O(1s) VBE for liquid water was 538.21 eV. An interesting finding by Olivieri et al. was that addition of 0.15 M BA shifted the O(1s) band for liquid water to 537.78 eV, from which they determined that the ionization energy for an aqueous solution depends on the composition of the solution.[23] The observed shift was striking because the O(1s) orbital is not expected to be much involved in intermolecular interactions. This led to the question of why the band was shifted.

Shown in Figure 7a are EUV photoelectron spectra of a 0.05 M aqueous NaCl solution with BA added at various

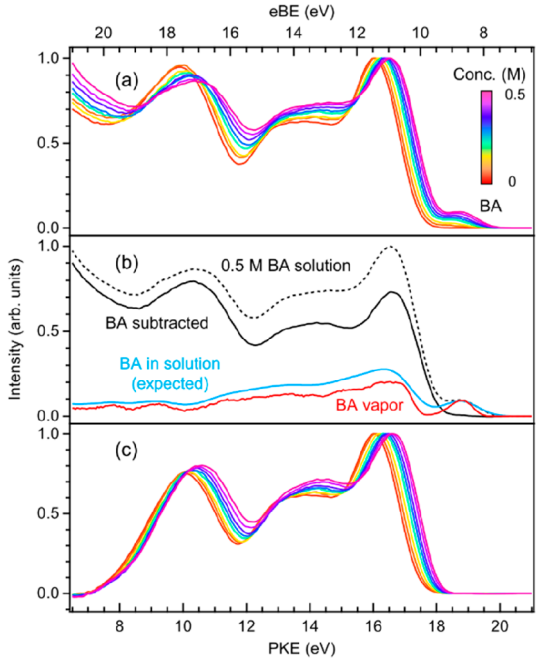

Figure 7. (a) Photoelectron spectra of 0.05 M aqueous NaCl solution with different BA concentrations. (b) Example of subtraction of BA signal for 0.5 M BA solution. The photoelectron spectrum of BA in solution (blue) was estimated by convoluting the spectrum (red) of BA vapor with a Gaussian function and subtracted from the overall spectrum of the solution. See the text. (c) Spectra after subtraction of BA and background photoemission signals.

concentrations. A small amount of NaCl was dissolved in the solution to stabilize the streaming potential of the liquid microjet. It can be seen that the VIE for liquid water clearly decreases with increasing BA concentration and is reduced by 0.4 eV for a BA concentration of 0.15 M. This result is consistent with that of Olivieri et al., who found that the O(1s) photoelectron band position depended on the BA concentration, indicating that the entire photoemission spectrum

https://doi.org/10.1021/acs.jpcb.1c04765
J. Phys. Chem. B 2021, 125, 10514−10526

including the inner-shell and valence bands for liquid water is shifted by the potential of the solution. It is also noted here that the probing depth of photoemission spectroscopy depends on the electron kinetic energy. Olivieri et al. employed a photon energy greater than 800 eV, which provided a PKE of about 300 eV, while our experiment gave a PKE of about 20 eV. According to previous estimates, the electron attenuation length in liquid water is different by at least a factor of 2−4 for eKEs of 20 and 300 eV.[11] However, a similar eBE shift is seen independent of the probing depth because the surface dipole moment created by segregated BA is located outside the bulk solution, as shown in Figure 15.

For a more detailed spectroscopic analysis of solvent water in aqueous BA solutions, we attempted subtracting the spectrum of hydrated BA from the observed photoelectron spectra of BA solutions. Because the photoelectron spectrum of hydrated BA cannot be measured separately, we estimated it from the spectrum of gaseous BA in the following way. As seen in Figure 7a, the first photoelectron band of hydrated BA is isolated at VBE of about 9 eV. Therefore, we measured the photoelectron spectrum of gaseous BA, as shown in Figure 7b, and compared the spectral bandwidth of the first band between aqueous BA solution and gaseous BA. This comparison indicated that the spectral broadening in solution is expressed with a Gaussian function with a FWHM of 1 eV. Thus, we convoluted the spectrum of BA vapor with the Gaussian to predict the entire photoelectron spectrum of hydrated BA as shown in Figure 7b. (The relative band positions and intensities were assumed to be unaltered by solvation.) Finally, we subtracted this spectrum from the photoelectron spectrum of the BA solution to extract the spectral features of solvent water as shown in Figure 7c. The band positions of liquid water thus estimated are summarized in Figure 8a, where it can be seen that all VBE values decrease with increasing BA concentration. These shifts seem to be almost proportional to the interfacial BA concentration, estimated from the photoelectron intensity, shown in Figure 8b, and they gradually saturate. BA is an amphiphilic compound, and it is expected to segregate at the gas−liquid interface. The relative shift from the $1b_1$ band position is plotted in Figure 8c, and the FWHM values obtained by fitting are shown in Figure 8d.

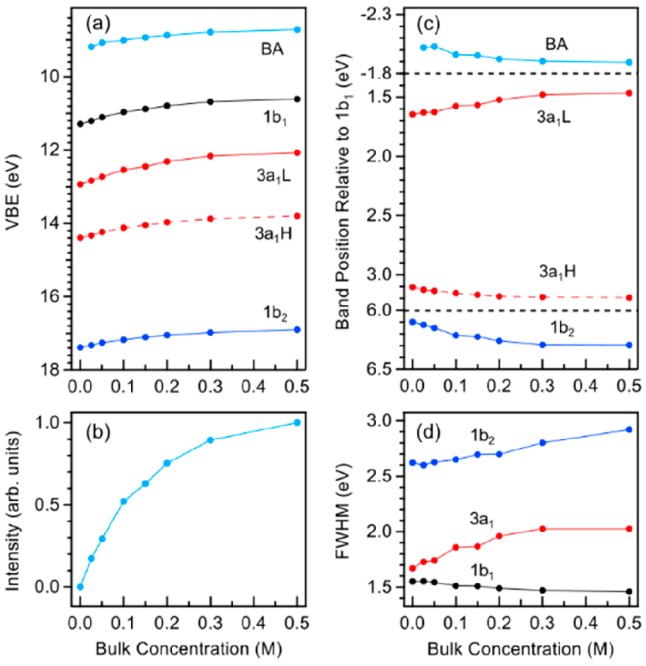

Figure 8. (a) VBE measured for different bands of aqueous BA solutions. 50 mM of NaCl was added. (b) BA band intensity relative to that for $1b_1$. (c) Band position relative to that for $1b_1$. (d) FWHM for each band. The experimental uncertainty is ±0.05 eV, which is the instrumental resolution.

Given that BA is segregated at the gas−liquid interface, photoelectrons emitted from the solvent water may be inelastically scattered by this interfacial BA. Although this cannot be ruled out, inelastic scattering would be expected to reduce the PKE and increase the apparent eBE at higher BA concentration, which is opposite to what we observe. Therefore, the upshift of the PKE with increasing BA concentration is not due to scattering but is an electronic effect. We performed molecular dynamics simulations for a BA aqueous solution, in which the bulk BA concentration was assumed to be 10, 20, or 24 mM, and the surface concentration was calculated to be ∼5 M. For these bulk concentrations, the surface potential was estimated to be −0.66, −0.68, and −0.74 V, which are greater than that for pure water (−0.63 V) by −0.03, −0.05, and −0.11 V, respectively. The magnitude and polarity of the computed surface potentials are in reasonable agreement with the −0.1 eV shift in VIE experimentally observed for a BA concentration of 50 mM.

Because BA is an amine, it is of interest to change the pH to produce the protonated form (BAH^+) and examine its influence. The pK_a value for a conjugated acid of BA in liquid water is 10.8. As shown in Figure 9, the pH of an aqueous solution of 0.5 M BA and 50 mM NaCl is expected to decrease from 11 to 6 as the HCl concentration is increased from 0.1 to 0.5 M, and the fraction of BAH^+ in an aqueous solution of 0.5 M BA and 50 mM NaCl is expected to increase from 0.2 to about 1.0 as the HCl concentration is increased from 0.1 to 0.5 M. Figure 10a shows photoelectron spectra measured for various HCl concentrations. The spectra shown in Figure 10b were obtained by subtracting the contributions of BA and BAH^+ by least-squares fitting. In our analysis, BA and BAH^+ were not differentiated, and the bands were fit by shifting the aforementioned broadened photoelectron spectrum of gaseous BA. As seen in Figure 10c, the VIE for both liquid water and BA gradually increases with increasing HCl concentration. The

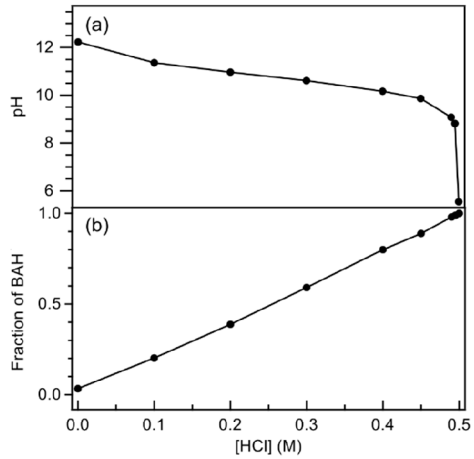

Figure 9. Calculated (a) pH value and (b) fraction of BAH^+ as a function of HCl concentration.

https://doi.org/10.1021/acs.jpcb.1c04765
J. Phys. Chem. B 2021, 125, 10514−10526

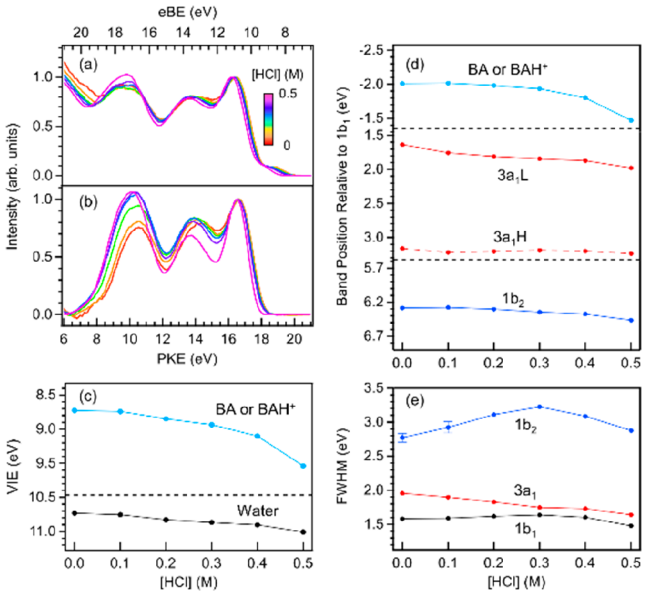

Figure 10. (a) Measured photoelectron spectra of aqueous solutions of 0.5 M BA and 50 mM NaCl as a function of HCl concentration. (b) Spectra in (a) after subtraction of solute and background signals. (c) Spectral shifts of BA/BAH^+ and $1b_1$ bands at each HCl concentration. (d) Band positions relative to $1b_1$ band. (e) FWHM of individual bands. In (c−e), the error bars are indicated only when the fitting errors exceed ±0.05 eV; otherwise, the experimental uncertainty is ±0.05 eV, which is the instrumental resolution.

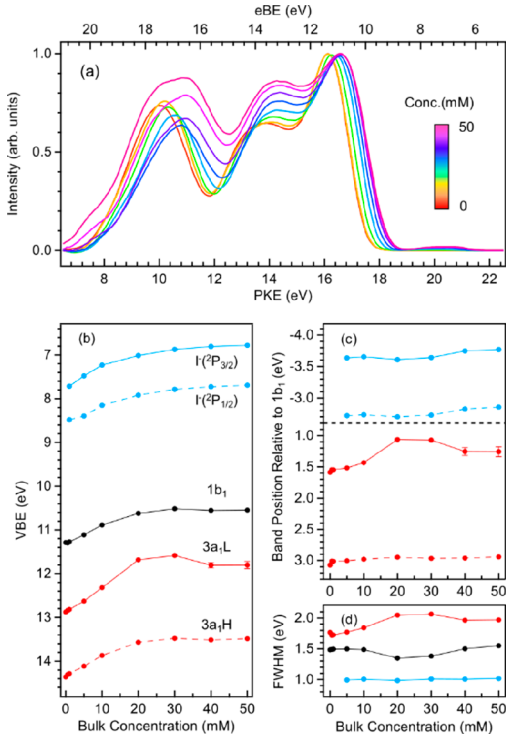

Figure 11. Variation of photoelectron spectrum of aqueous TBAI solution. (a) Photoelectron spectra, (b) VBE for individual bands, (c) relative energy shift from $1b_1$ band, and (d) FWHM. In (b−d), the experimental uncertainty estimated from the instrumental resolution is ±0.05 eV. The estimated values vary smoothly with concentration, although the values for 20 and 30 mM are slightly off. The photoelectron band of TBA^+ is anticipated at around the $1b_2$ band, but it is not considered in the fitting. Therefore, the $1b_2$ band is excluded from these plots.

relative band positions shown in Figure 10d reveal that the degree of $3a_1$ band splitting decreases with increasing HCl concentration. The BA band position shifts slightly with increasing HCl concentration, which is ascribed to protonation of BA. The FWHM's calculated by the least-squares fitting are also shown in Figure 10e.

Aqueous Solution of Tetrabutylammonium Iodide (TBAI). An aqueous TBAI solution is known to form EDL of segregated TBA^+ and dragged I^- ions at the gas−liquid interface. N(1s) photoemission spectroscopy of aqueous TBAI solution revealed that the density of TBA^+ is 66 times higher at the gas−liquid interface than that in the bulk,[20] and the I^- photoemission intensity for an aqueous TBAI solution was found to be 70 times higher.[22] Figure 11a shows photoelectron spectra of aqueous TBAI solutions for various concentrations up to 50 mM. Given the above-mentioned surface density increase of about 70 times, the highest bulk concentration of 50 mM gives a surface TBA^+ concentration of 3.5 M. The spectra clearly indicate that the VIE for liquid water decreases with increasing TBAI concentration. At similar concentrations of 3−5 M, an aqueous NaI solution does not exhibit as large a VIE shift as seen here. An aqueous TBAI solution exhibits a photoelectron band due to TBA^+ in the vicinity of the $1b_2$ band, which makes spectral analysis of this region more complex and less reliable. We focus on the $I^-5p(^2P_J)$, $1b_1$, and $3a_1$ bands here, similarly with other cases. Figure 11b shows the absolute VBE values for these bands. All bands shift to lower VBE values with increasing TBAI concentration, indicating that the entire photoemission spectrum is shifted due to the TBAI EDL. These shifts become saturated as the I^- density in the interfacial region saturates. To examine the individual band shifts, Figure 11c presents the relative band positions measured from the $1b_1$ band. Figure 11d shows the FWHM of these bands. Although the values at 20 and 30 mM are slightly off, the estimated values change smoothly with the concentration.

The observation of a spectral shift for aqueous TBAI solutions warrants reconsideration of our previous TRPES results for CTTS reactions in aqueous TBAI solutions.[20,21] Previously, we compared TARPES results for CTTS reactions in aqueous 0.5 M NaI and 50 mM TBAI solutions and found that the eBE values in the latter were much lower than in the former.[21] We then investigated CTTS in aqueous TBAI solutions in more detail for a wider concentration range and found that the dynamics in the TBAI concentration range of 0.1−1 mM were essentially the same as those in NaI solutions but that the CTTS kinetic rate constants and the eBE values for the CTTS state and hydrated electrons (e_{aq}^-) change dramatically at higher concentrations.[20] We attributed the reduction in the VBE for e_{aq}^- to electron trapping in regions with high solute concentration. However, the present study indicates that the entire photoemission spectrum of an aqueous TBAI solution is shifted, including the bands for liquid water and I^-. Thus, the spectral shift for e_{aq}^- in aqueous TBAI solutions at high concentration is most likely due to the effect of the surface dipole moment.[69] The clear photoemission signal observed for I^- indicates that the probing depth of our EUV photoemission spectroscopy is comparable to or greater than the average depth of I^-. Because the electric potential of the liquid steeply changes between these layers of TBA^+ and I^-, chemical species located at smaller depths than I^- will exhibit smaller VBE shifts than that of I^-; the VBE shift of

https://doi.org/10.1021/acs.jpcb.1c04765
J. Phys. Chem. B 2021, 125, 10514−10526

TBA^+, measurable by using N(1s) photoemission spectroscopy, is possibly smaller than that of I^-. As shown in Figure 12,

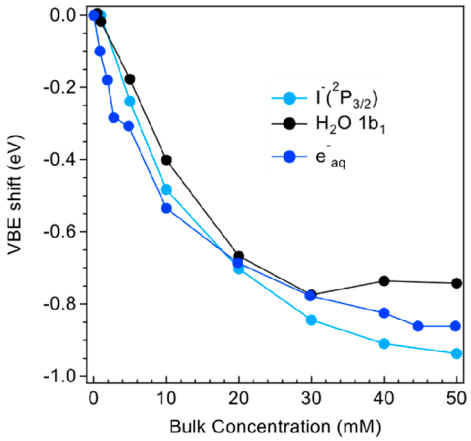

Figure 12. VBE shift for I^-, $1b_1$ of water, and hydrated electron bands in aqueous TBAI solutions with various concentrations. The values for hydrated electron are taken from ref 20.

the VBE shifts observed for $1b_1$ of liquid water and e_{aq}^- [20] are similar. The results suggest that the observed signals of water and e_{aq}^- do not originate from the region at much smaller depths than that of I^-. We are currently revisiting the CTTS reaction in aqueous TBAI solutions using EUV-TRPES to confirm the VBE shift of e_{aq}^- determined by UV-TRPES.

Aqueous Sodium Butyrate Solution. Because TBA^+ and BA are cationic and neutral compounds, it is interesting to examine anionic compounds. Sodium butyrate (SB) dissociates into Na^+ and butyrate anions. The photoelectron spectra of aqueous SB solutions are shown in Figure 13a. The results indicate that the spectral shift is very small. As seen in Figure 13b,c, the influence of this solute on the photoelectron spectra of liquid water is quite small.

Methanol Solutions of NaI. Figure 14a shows photoelectron spectra of methanol solutions of NaI up to a concentration of 3 M. The 7a′ band reveals the most prominent spectral variation with changing concentration, reminiscent of the $3a_1$ band of liquid water. Thus, we analyzed the 7a′ band as a combination of two split bands. Similar to the $1b_2$ band of liquid water, the experimental result on the 5a′ band is less accurate because of an overlap with a low-energy background, so that we exclude it from our discussion and only indicate its estimated band position. The 6a′/1a″ band is taken into consideration to evaluate the 7a′ band positions accurately, in which the 6a′/1a″ band is approximated as a single band. More detailed discussion about the valence bands of liquid methanol can be found elsewhere.[15] We performed least-squares fitting of the spectra by assuming the same Gaussian shape for both of the split 7a′ bands. Figure 14b–f shows the concentration dependence of the photoelectron band position obtained by this analysis. The VIE value determined from the 2a″ band position was almost constant for different NaI concentrations (Figure 14c). The degree of splitting of the 7a′ band decreases with increasing concentration, similar to the $3a_1$ band for liquid water; however, both of the 7a′H and 7a′L shift in this case (Figure 14d). The FWHM values estimated by the least-squares fitting have relatively large uncertainties, and they are indicated as colored bands in Figure 14g. However, the ratio of the integrated

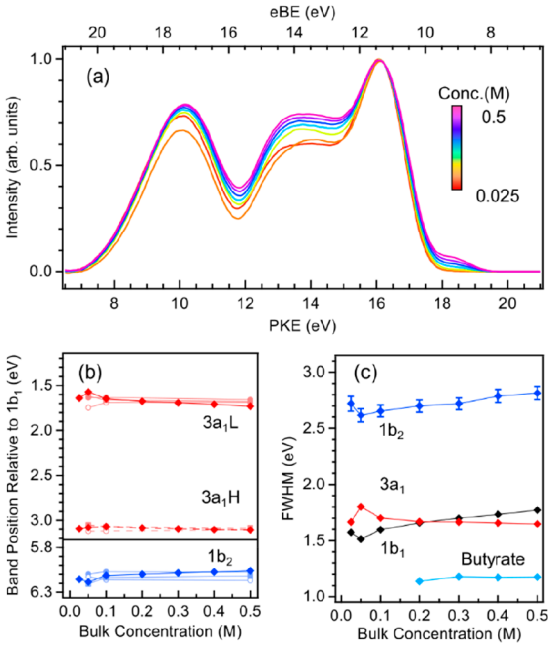

Figure 13. Variation of photoelectron spectrum of aqueous sodium butyrate solution. (a) Photoelectron spectra, (b) relative energy shift from $1b_1$ band, and (c) FWHM. Pale color symbols in (b) are band positions for NaX (X = Cl, I, OH). In (b, c), the error bars are indicated only when the fitting errors exceed ±0.05 eV; otherwise, the experimental uncertainty is ±0.05 eV, which is the instrumental resolution.

intensities 7a′/2a″ estimated by our analysis was constant in the entire concentration range, so that the results are reasonable from that point of view. The low solubility of NaCl in methanol prevented us from performing similar measurements, so the effect of the halogen anions could not be examined for methanol.

DISCUSSION

Overall Energy Shift. When the surface potential χ in eq 1 moves toward the negative direction, electrons emitted from the liquid surface gain an additional kinetic energy upon ejection into the vacuum. This energy shift is the same for all electrons irrespective of the nature (inner-shell or valence) of an electron orbital or the emitter (solute or solvent), except for photoelectrons generated above the EDL. Our EUV photoemission spectroscopy results for the valence bands of liquid water support the earlier observations by Olivieri et al. that the O(1s) photoelectron energy is shifted due to the addition of BA. The present study demonstrates that these energy shifts are consistent with the surface potentials computed by using molecular dynamics simulations.

Strong electrolytes, such as NaCl and NaI, do not induce appreciable energy shifts in the photoemission spectrum even at high concentrations on the order of a few mol/L. Solutes such as TBAI and BA, segregated or preferentially adsorbed at the interfacial region, cause an energy shift that is almost proportional to the surface solute density. To clarify the origin of these surface potentials, we present a few representative depth profiles of solutes in Figure 15a–f and calculated surface potentials in Figure 15g, h. In the case of BA, its alkyl group is hydrophobic, and it induces segregation of BA at the liquid surface with NH_2 embedded in the bulk and the alkyl group exposed to the vacuum. Thus, the dipole moment of BA (0.294

https://doi.org/10.1021/acs.jpcb.1c04765
J. Phys. Chem. B 2021, 125, 10514–10526

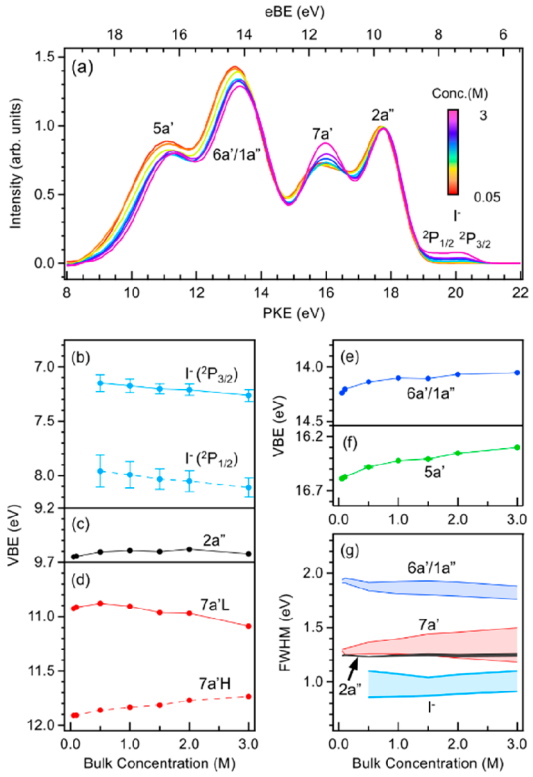

Figure 14. (a) Photoelectron spectra of methanol solutions of NaI. Concentration dependence of spectral shift for (b) I^- (light blue), (c) 2a″ (black), (d) 7a′ (red), (e) 1a″ and 6a′ (blue), and (f) 5a′ (green). (g) Variation of FWHM with concentration. The FWHM values are associated with relatively large uncertainties, and they are indicated as colored bands. In (b–f), the error bars are indicated only when the fitting errors exceed ±0.05 eV; otherwise, the experimental uncertainty is ±0.05 eV, which is the instrumental resolution.

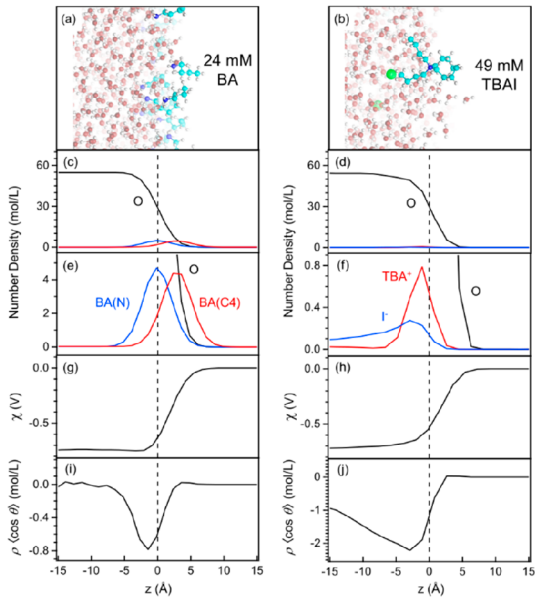

Figure 15. Computed structures and electric potential at the gas–liquid interfaces of aqueous 24 mM BA and 49 mM TBAI solutions. (a, b) Snapshot of molecular dynamics simulation at the gas–liquid interface, (c, d) depth profiles of solutes, (e, f) enlarged view of depth profiles, (g, h) electric potential, and (i, j) $\rho\langle\cos\theta\rangle$ computed for aqueous BA and TBAI solutions, respectively. The dashed vertical line indicates the Gibbs dividing surface. In (a, b), H, O, C, N, and I^- atoms are indicated in white, red, cyan, blue, and green, respectively.

D) creates an electric field that is a primary source for the negative potential of the liquid. When HCl is added to an aqueous BA solution, BA is protonated, and its spatial distribution extends into the bulk. The Cl^- counterions are distributed beneath the BAH^+. The EDL orients the water molecules in this region, which compensates in part for the dipole moment created by the EDL. The orientational distribution of water molecules is shown in Figure 15i, j, and the degree of orientation is seen to be stronger in aqueous TBAI than in a BA solution.

Band Shift and Splitting. EUV photoemission spectra of solutions revealed a clear variation of the relative energy and shape of photoelectron bands as a function of solute concentration. Because the photoelectron bands for solutes are very weak and are only observable in the eBE region lower than the VIE for the solvent, only a small number of solute bands could be observed. Nevertheless, energy shifts were identified for the photoelectron bands for solutes.

The photoelectron spectra of aqueous NaCl, NaI, and NaOH solutions exhibited a reduced splitting width of the $3a_1$ band. A similar feature was also seen for the 7a′ band of liquid methanol in NaI solution. As a solute concentration increases, a greater number of solvent molecules are involved in the solvation shell of ions. In an aqueous NaI solution, for example, each Na^+ ion binds 5–6 water molecules on average in its first hydration shell[70] and similarly each I^- ion has 6–7 water molecules;[43,71] therefore, in the aqueous 5 M NaI solution, each water molecule interacts with at least one of Na^+ or I^-. Thus, a fraction of intact water molecules with a double donor and double acceptor configuration considerably diminish at high concentrations; the splitting of $3a_1$ never vanishes while its splitting magnitude changes in altered hydrogen-bonding structures. The change of intermolecular distances is another possible source for variation of the $3a_1$ splitting width that is caused by intermolecular orbital interactions. However, molecular dynamics simulations seem to indicate that the radial distribution functions of the O–O distance in an aqueous NaCl solution is not noticeably altered from that in pure water.[43,72] A full interpretation of the concentration dependence of the photoelectron spectra of solutions requires detailed quantum chemical simulations of solute–solvent interactions and photoemission processes, which is beyond the scope of this study. Previously, Pohl et al. performed theoretical simulations of photoelectron spectra of aqueous NaI solutions by using quantum chemical treatment of an ionized water molecule and its first hydration shell surrounded by a dielectric continuum.[18] Further extensive quantum mechanical simulations of photoemission of solutions are indispensable for extracting as much information as possible from the experimental results.

TBAI induced much smaller changes in the $3a_1$ band splitting. One possible explanation for it is that TBA^+ has a weaker influence than Na^+ on the hydrogen-bonding structure of liquid water. Another possibility is that there is a large contribution of the photoelectron spectrum of liquid water from the deeper region, where TBAI concentration is much lower than that in EDL. The clear observation of the photoelectron signal for I^- indicates that the probing depth of EUV photoemission spectroscopy is comparable with or greater than the width of EDL. (Olivieri et al. estimated the

https://doi.org/10.1021/acs.jpcb.1c04765
J. Phys. Chem. B 2021, 125, 10514–10526

inelastic mean free path (IMFP) of an electron in aqueous NaI solution for eKE between 65 and 1500 eV, in which IMFP was estimated to be less than 1 nm in the energy region less than 100 eV.[73]) We speculate that both of the above two factors are operative here. In the case of BA, BA resides outside of liquid, so that BA shifts the entire photoemission spectra while the influence on the spectral features of liquid water is weak.

In this study, we have discussed the valence bands of the solvents and solutes by subtracting the low-energy background signal from the observed spectrum, as shown in Figure 1. However, it is worth noting that the relative intensity of the low-energy background signal to the valence bands increased with a solute concentration in all cases (e.g., Figures 7a and 10a). This fact implies that the presence of solute alters the efficiency of dynamical processes, such as elastic/inelastic scattering and intermolecular Coulombic decay, responsible for the background signal. Explanation of the concentration-dependent background signal will be challenging but helpful for deepening our understanding of electron transport in liquids.

The influence of ions on the hydrogen-bonding network is phenomenologically related to the Hoffmeister series for precipitation of proteins and the arguments of structure maker and breaker for liquid water. It is of great interest to further explore ion−solvent interactions and also hydrophobic hydration by using photoemission spectroscopy and quantum chemical calculations.

CONCLUSION

We investigated photoemission spectra of aqueous solutions of various electrolytes and a methanol solution of NaI. Strong inorganic electrolytes do not significantly alter the VIE for solvents even at high concentrations, while they influence the photoelectron bands for electron orbitals relevant to the hydrogen-bonding network of solvent molecules. Hydrophobic organic solutes such as TBA^+ and BA are concentrated at the interfacial region, and they induce an appreciable VIE shift for liquid water at relatively low concentrations. These effects are due to the formation of surface dipoles, but the mechanisms are slightly different between BA and TBAI. BA is electrically neutral and has an amino group embedded in the liquid and a butyl group on the vacuum side to orient its permanent dipole nearly normal to the surface. BA does not cause strong orientation of water molecules. TBA^+ is at the surface of the liquid, and it drags its counterion I^- underneath the TBA-rich layer to form an EDL. Water molecules in the EDL are strongly oriented with their permanent dipole moment antiparallel to the electric field and the hydrogen atoms pointing away from the surface. The unquenched electric field in the EDL shifts the surface potential of aqueous solutions. The observed shifts of eBE values agree with classical molecular dynamics simulations. The splitting of the $3a_1$ band of liquid water and the 7a′ band of liquid methanol indicates the influence of a solute on the hydrogen-bonding network of the solvents. Quantum chemical calculations are necessary to elucidate the atomistic mechanisms that alter the photoelectron spectra.

This study showed that photoemission spectroscopy of liquids can provide useful information for investigating the electronic structures and molecular interactions at a gas−liquid interface. It is desirable to improve the energy resolution of a MBTOF spectrometer by the use of a larger flight length, and such modification of our apparatus is in progress. At present, the probing depth of photoemission spectroscopy of liquids is not precisely known and is estimated to be about a nanometer. When the probing depth is determined more accurately, photoemission spectroscopy will provide further insights into interfacial molecular structures and distributions. Previously, we reported TARPES using UV probe pulses. Although TARPES using EUV radiation is technically rather demanding, it will be highly useful for studying gas−liquid interfaces. The use of a tabletop soft X-ray laser will also expand the opportunities of this approach.

ASSOCIATED CONTENT

Supporting Information

The Supporting Information is available free of charge at https://pubs.acs.org/doi/10.1021/acs.jpcb.1c04765.

Energy calibration method and molecular dynamics simulation (PDF)

AUTHOR INFORMATION

Corresponding Author

Toshinori Suzuki − *Department of Chemistry, Graduate School of Science, Kyoto University, Kyoto 606-8502, Japan;* orcid.org/0000-0002-4603-9168; Email: suzuki@kuchem.kyoto-u.ac.jp

Authors

Yo-ichi Yamamoto − *Department of Chemistry, Graduate School of Science, Kyoto University, Kyoto 606-8502, Japan*

Tatsuya Ishiyama − *Department of Applied Chemistry, Graduate School of Science and Engineering, University of Toyama, Toyama 930-8555, Japan;* orcid.org/0000-0003-2388-7727

Akihiro Morita − *Department of Chemistry, Graduate School of Science, Tohoku University, Sendai 980-8578, Japan; Elements Strategy Initiative for Catalysts and Batteries (ESICB), Kyoto University, Kyoto 615-8530, Japan;* orcid.org/0000-0002-2104-0605

Complete contact information is available at: https://pubs.acs.org/10.1021/acs.jpcb.1c04765

Notes

The authors declare no competing financial interest.

ACKNOWLEDGMENTS

This work was supported by the JSPS KAKENHI Grants (Nos. 21H04970, 21H01878, 20H00368, and 18H05265), the Mitsubishi Foundation, the Fugaku Supercomputer Project (No. JPMXP1020200308) from the Ministry of Education, Culture, Sports, Science and Technology of Japan, and the Asahi Glass Foundation. Some of the molecular dynamics simulations in this study were performed by using the supercomputers at the Research Center for Computational Science of National Institutes of Natural Sciences and MASAMUNE-IMR at Center for Computational Material Science of Tohoku University. We thank Professor Nobuhiro Kosugi for his helpful comments on the manuscript. The data presented here are available on request sent to suzuki@kuchem.kyoto-u.ac.jp.

REFERENCES

(1) Marcus, Y. Effect of Ions on the Structure of Water: Structure Making and Breaking. *Chem. Rev.* **2009**, *109*, 1346−1370.

(2) Ohtaki, H.; Radnai, T. Structure and Dynamics of Hydrated Ions. *Chem. Rev.* **1993**, *93*, 1157−1204.
(3) Frank, H. S.; Wen, W. Y. Structural Aspects of Ion-Solvent Interaction in Aqueous Solutions: A Suggested Picture of Water Structure. *Discuss. Faraday Soc.* **1957**, *24*, 133−140.
(4) Omta, A. W.; Kropman, M. F.; Woutersen, S.; Bakker, H. J. Negligible Effect of Ions on the Hydrogen-Bond Structure in Liquid Water. *Science* **2003**, *301*, 347−349.
(5) Zhang, Y. J.; Cremer, P. S. Interactions between Macromolecules and Ions: The Hofmeister Series. *Curr. Opin. Chem. Biol.* **2006**, *10*, 658−663.
(6) Jungwirth, P.; Tobias, D. J. Specific Ion Effects at the Air/Water Interface. *Chem. Rev.* **2006**, *106*, 1259−1281.
(7) Berendsen, H. J. C.; Grigera, J. R.; Straatsma, T. P. The Missing Term in Effective Pair Potentials. *J. Phys. Chem.* **1987**, *91*, 6269−6271.
(8) Faubel, M.; Steiner, B.; Toennies, J. P. Photoelectron Spectroscopy of Liquid Water, Some Alcohols, and Pure Nonane in Free Micro Jets. *J. Chem. Phys.* **1997**, *106*, 9013−9031.
(9) Winter, B.; Faubel, M. Photoemission from Liquid Aqueous Solutions. *Chem. Rev.* **2006**, *106*, 1176−1211.
(10) Dupuy, R.; Richter, C.; Winter, B.; Meijer, G.; Schlögl, R.; Bluhm, H. Core Level Photoelectron Spectroscopy of Heterogeneous Reactions at Liquid-Vapor Interfaces: Current Status, Challenges, and Prospects. *J. Chem. Phys.* **2021**, *154*, 060901.
(11) Suzuki, T. Ultrafast Photoelectron Spectroscopy of Aqueous Solutions. *J. Chem. Phys.* **2019**, *151*, 090901.
(12) Buttersack, T.; Mason, P. E.; McMullen, R. S.; Schewe, H. C.; Martinek, T.; Brezina, K.; Crhan, M.; Gomez, A.; Hein, D.; Wartner, G.; et al. Photoelectron Spectra of Alkali Metal-Ammonia Microjets: From Blue Electrolyte to Bronze Metal. *Science* **2020**, *368*, 1086−1091.
(13) Jordan, I.; Huppert, M.; Rattenbacher, D.; Peper, M.; Jelovina, D.; Perry, C.; von Conta, A.; Schild, A.; Wörner, H. J. Attosecond Spectroscopy of Liquid Water. *Science* **2020**, *369*, 974−979.
(14) Kurahashi, N.; Karashima, S.; Tang, Y.; Horio, T.; Abulimiti, B.; Suzuki, Y. I.; Ogi, Y.; Oura, M.; Suzuki, T. Photoelectron Spectroscopy of Aqueous Solutions: Streaming Potentials of NaX (X = Cl, Br, and I) Solutions and Electron Binding Energies of Liquid Water and X^-. *J. Chem. Phys.* **2014**, *140*, 174506.
(15) Thürmer, S.; Shinno, T.; Suzuki, T. Valence Photoelectron Spectra of Liquid Methanol and Ethanol Measured Using He II Radiation. *J. Phys. Chem. A* **2021**, *125*, 2492−2503.
(16) Faubel, M.; Steiner, B. Strong Bipolar Electrokinetic Charging of Thin Liquid Jets Emerging from 10 μm PtIr Nozzles. *Ber. Bunsen. Phys. Chem.* **1992**, *96*, 1167−1172.
(17) Preissler, N.; Buchner, F.; Schultz, T.; Lübcke, A. Electrokinetic Charging and Evidence for Charge Evaporation in Liquid Microjets of Aqueous Salt Solution. *J. Phys. Chem. B* **2013**, *117*, 2422−2428.
(18) Pohl, M. N.; Muchová, E.; Seidel, R.; Ali, H.; Sršeá, S.; Wilkinson, I.; Winter, B.; Slavíček, P. Do Water's Electrons Care About Electrolytes? *Chem. Sci.* **2019**, *10*, 848−865.
(19) Thürmer, S.; Malerz, S.; Trinter, F.; Hergenhahn, U.; Lee, C.; Neumark, D. M.; Meijer, G.; Winter, B.; Wilkinson, I. Accurate Vertical Ionization Energy and Work Function Determinations of Liquid Water and Aqueous Solutions. *Chem. Sci.* **2021**, *12*, 10558−10582.
(20) Karashima, S.; Suzuki, T. Charge-Transfer-to-Solvent Reaction in a Hydrophobic Tetrabutylammonium Iodide Molecular Layer in Aqueous Solution. *J. Phys. Chem. B* **2019**, *123*, 3769−3775.
(21) Yamamoto, Y.; Suzuki, Y. I.; Tomasello, G.; Horio, T.; Karashima, S.; Mitríc, R.; Suzuki, T. Time- and Angle-Resolved Photoemission Spectroscopy of Hydrated Electrons near a Liquid Water Surface. *Phys. Rev. Lett.* **2014**, *112*, 187603.
(22) Winter, B.; Weber, R.; Schmidt, P. M.; Hertel, I. V.; Faubel, M.; Vrbka, L.; Jungwirth, P. Molecular Structure of Surface-Active Salt Solutions: Photoelectron Spectroscopy and Molecular Dynamics Simulations of Aqueous Tetrabutylammonium Iodide. *J. Phys. Chem. B* **2004**, *108*, 14558−14564.
(23) Olivieri, G.; Goel, A.; Kleibert, A.; Cvetko, D.; Brown, M. A. Quantitative Ionization Energies and Work Functions of Aqueous Solutions. *Phys. Chem. Chem. Phys.* **2016**, *18*, 29506−29515.
(24) Nishizawa, K.; Kurahashi, N.; Sekiguchi, K.; Mizuno, T.; Ogi, Y.; Horio, T.; Oura, M.; Kosugi, N.; Suzuki, T. High-Resolution Soft X-Ray Photoelectron Spectroscopy of Liquid Water. *Phys. Chem. Chem. Phys.* **2011**, *13*, 413−417.
(25) Weber, R.; Winter, B.; Schmidt, P. M.; Widdra, W.; Hertel, I. V.; Dittmar, M.; Faubel, M. Photoemission from Aqueous Alkali-Metal-Iodide Salt Solutions Using EUV Synchrotron Radiation. *J. Phys. Chem. B* **2004**, *108*, 4729−4736.
(26) Tissot, H.; Gallet, J. J.; Bournel, F.; Olivieri, G.; Silly, M. G.; Sirotti, F.; Boucly, A.; Rochet, F. The Electronic Structure of Saturated NaCl and NaCl Solutions in Contact with a Gold Substrate. *Top. Catal.* **2016**, *59*, 605−620.
(27) Ishii, H.; Sugiyama, K.; Ito, E.; Seki, K. Energy Level Alignment and Interfacial Electronic Structures at Organic Metal and Organic Organic Interfaces. *Adv. Mater.* **1999**, *11*, 605−625.
(28) Jablonski, A.; Powell, C. J. Effective Attenuation Lengths for Different Quantitative Applications of X-Ray Photoelectron Spectroscopy. *J. Phys. Chem. Ref. Data* **2020**, *49*, 033102.
(29) Shinotsuka, H.; Tanuma, S.; Powell, C. J.; Penn, D. R. Calculations of Electron Inelastic Mean Free Paths. XII. Data for 42 Inorganic Compounds over the 50 eV to 200 keV Range with the Full Penn Algorithm. *Surf. Interface Anal.* **2019**, *51*, 427−457.
(30) Shen, Y. R. *Fundamentals of Sum-Frequency Spectroscopy*; Cambridge University Press: Cambridge, 2016.
(31) Eisenthal, K. B. Liquid Interfaces Probed by Second-Harmonic and Sum-Frequency Spectroscopy. *Chem. Rev.* **1996**, *96*, 1343−1360.
(32) Richmond, G. L. Molecular Bonding and Interactions at Aqueous Surfaces as Probed by Vibrational Sum Frequency Spectroscopy. *Chem. Rev.* **2002**, *102*, 2693−2724.
(33) Nihonyanagi, S.; Mondal, J. A.; Yamaguchi, S.; Tahara, T. Structure and Dynamics of Interfacial Water Studied by Heterodyne-Detected Vibrational Sum-Frequency Generation. *Annu. Rev. Phys. Chem.* **2013**, *64*, 579−603.
(34) Zhao, X. L.; Ong, S. W.; Wang, H. F.; Eisenthal, K. B. New Method for Determination of Surface pK_a Using Second Harmonic Generation. *Chem. Phys. Lett.* **1993**, *214*, 203−207.
(35) Kruit, P.; Read, F. H. Magnetic Field Parallelizer for 2π Electron-Spectrometer and Electron-Image Magnifier. *J. Phys. E: Sci. Instrum.* **1983**, *16*, 313−324.
(36) Ojeda, J.; Arrell, C. A.; Longetti, L.; Chergui, M.; Helbing, J. Charge-Transfer and Impulsive Electronic-to-Vibrational Energy Conversion in Ferricyanide: Ultrafast Photoelectron and Transient Infrared Studies. *Phys. Chem. Chem. Phys.* **2017**, *19*, 17052−17062.
(37) Engel, N.; Bokarev, S. I.; Moguilevski, A.; Raheem, A. A.; Al-Obaidi, R.; Möhle, T.; Grell, G.; Siefermann, K. R.; Abel, B.; Aziz, S. G.; et al. Light-Induced Relaxation Dynamics of the Ferricyanide Ion Revisited by Ultrafast XUV Photoelectron Spectroscopy. *Phys. Chem. Chem. Phys.* **2017**, *19*, 14248−14255.
(38) Hummert, J.; Reitsma, G.; Mayer, N.; Ikonnikov, E.; Eckstein, M.; Kornilov, O. Femtosecond Extreme Ultraviolet Photoelectron Spectroscopy of Organic Molecules in Aqueous Solution. *J. Phys. Chem. Lett.* **2018**, *9*, 6649−6655.
(39) Nishitani, J.; Yamamoto, Y.; West, C. W.; Karashima, S.; Suzuki, T. Binding Energy of Solvated Electrons and Retrieval of True UV Photoelectron Spectra of Liquids. *Sci. Adv.* **2019**, *5*, aaw6896.
(40) Matsumoto, M.; Kataoka, Y. Study on Liquid Vapor Interface of Water. I. Simulational Results of Thermodynamic Properties and Orientational Structure. *J. Chem. Phys.* **1988**, *88*, 3233−3245.
(41) Wilson, M. A.; Pohorille, A.; Pratt, L. R. Comment on "Study on the Liquid Vapor Interface of Water. I. Simulation Results of Thermodynamic Properties and Orientational Structure. *J. Chem. Phys.* **1989**, *90*, 5211−5213.
(42) Sokhan, V. P.; Tildesley, D. J. The Free Surface of Water: Molecular Orientation, Surface Potential and Nonlinear Susceptibility. *Mol. Phys.* **1997**, *92*, 625−640.

(43) Ishiyama, T.; Morita, A. Molecular Dynamics Study of Gas-Liquid Aqueous Sodium Halide Interfaces. I. Flexible and Polarizable Molecular Modeling and Interfacial Properties. *J. Phys. Chem. C* **2007**, *111*, 721−737.
(44) Kurahashi, N.; Thürmer, S.; Liu, S. Y.; Yamamoto, Y.; Karashima, S.; Bhattacharya, A.; Ogi, Y.; Horio, T.; Suzuki, T. Design and Characterization of a Magnetic Bottle Electron Spectrometer for Time-Resolved Extreme UV and X-Ray Photoemission Spectroscopy of Liquid Microjets. *Struct. Dyn.* **2021**, *8*, 034303.
(45) Nishitani, J.; Karashima, S.; West, C. W.; Suzuki, T. Surface Potential of Liquid Microjet Investigated Using Extreme Ultraviolet Photoelectron Spectroscopy. *J. Chem. Phys.* **2020**, *152*, 144503.
(46) Nishitani, J.; West, C. W.; Suzuki, T. Angle-Resolved Photoemission Spectroscopy of Liquid Water at 29.5 eV. *Struct. Dyn.* **2017**, *4*, 044014.
(47) Siegbahn, H. Electron Spectroscopy for Chemical Analysis of Liquids and Solutions. *J. Phys. Chem.* **1985**, *89*, 897−909.
(48) Malerz, S.; Trinter, F.; Hergenhahn, U.; Ghrist, A.; Ali, H.; Nicolas, C.; Saak, C. M.; Richter, C.; Hartweg, S.; Nahon, L.; et al. Low-Energy Constraints on Photoelectron Spectra Measured from Liquid Water and Aqueous Solutions. *Phys. Chem. Chem. Phys.* **2021**, *23*, 8246−8260.
(49) Mucke, M.; Braune, M.; Barth, S.; Förstel, M.; Lischke, T.; Ulrich, V.; Arion, T.; Becker, U.; Bradshaw, A.; Hergenhahn, U. A Hitherto Unrecognized Source of Low-Energy Electrons in Water. *Nat. Phys.* **2010**, *6*, 143−146.
(50) Frassetto, F.; Cacho, C.; Froud, C. A.; Turcu, I. C. E.; Villoresi, P.; Bryan, W. A.; Springate, E.; Poletto, L. Single-Grating Monochromator for Extreme-Ultraviolet Ultrashort Pulses. *Opt. Express* **2011**, *19*, 19169−19181.
(51) Wang, J. M.; Wolf, R. M.; Caldwell, J. W.; Kollman, P. A.; Case, D. A. Development and Testing of a General Amber Force Field. *J. Comput. Chem.* **2004**, *25*, 1157−1174.
(52) Bayly, C. I.; Cieplak, P.; Cornell, W. D.; Kollman, P. A. A Well-Behaved Electrostatic Potential Based Method Using Charge Restraints for Deriving Atomic Charges - the RESP Model. *J. Phys. Chem.* **1993**, *97*, 10269−10280.
(53) Joung, I. S.; Cheatham, T. E. Determination of Alkali and Halide Monovalent Ion Parameters for Use in Explicitly Solvated Biomolecular Simulations. *J. Phys. Chem. B* **2008**, *112*, 9020−9041.
(54) Martínez, L.; Andrade, R.; Birgin, E. G.; Martínez, J. M. PACKMOL: A Package for Building Initial Configurations for Molecular Dynamics Simulations. *J. Comput. Chem.* **2009**, *30*, 2157−2164.
(55) Allen, M. P.; Tildesley, D. J. *Computer Simulation of Liquids*; Clarendon Press: Oxford, 1987.
(56) Hess, B.; Bekker, H.; Berendsen, H. J. C.; Fraaije, J. LINCS: A Linear Constraint Solver for Molecular Simulations. *J. Comput. Chem.* **1997**, *18*, 1463−1472.
(57) Nosé, S. A Unified Formulation of the Constant Temperature Molecular Dynamics Methods. *J. Chem. Phys.* **1984**, *81*, 511−519.
(58) Hoover, W. G. Canonical Dynamics: Equilibrium Phase-Space Distributions. *Phys. Rev. A: At., Mol., Opt. Phys.* **1985**, *31*, 1695−1697.
(59) Darden, T.; York, D.; Pedersen, L. Particle Mesh Ewald: An N·log(N) Method for Ewald Sums in Large Systems. *J. Chem. Phys.* **1993**, *98*, 10089−10092.
(60) Perera, L.; Essmann, U.; Berkowitz, M. L. Effect of the Treatment of Long-Range Forces on the Dynamics of Ions in Aqueous-Solutions. *J. Chem. Phys.* **1995**, *102*, 450−456.
(61) Van der Spoel, D.; Lindahl, E.; Hess, B.; Groenhof, G.; Mark, A. E.; Berendsen, H. J. C. GROMACS: Fast, Flexible, and Free. *J. Comput. Chem.* **2005**, *26*, 1701−1718.
(62) Kathmann, S. M.; Kuo, I. F. W.; Mundy, C. J.; Schenter, G. K. Understanding the Surface Potential of Water. *J. Phys. Chem. B* **2011**, *115*, 4369−4377.
(63) Winter, B.; Faubel, M.; Hertel, I. V.; Pettenkofer, C.; Bradforth, S. E.; Jagoda-Cwiklik, B.; Cwiklik, L.; Jungwirth, P. Electron Binding Energies of Hydrated H_3O^+ and OH^-: Photoelectron Spectroscopy of Aqueous Acid and Base Solutions Combined with Electronic Structure Calculations. *J. Am. Chem. Soc.* **2006**, *128*, 3864−3865.
(64) Radojević, V.; Kelly, H. P.; Johnson, W. R. Photodetachment of Negative Halogen Ions. *Phys. Rev. A: At., Mol., Opt. Phys.* **1987**, *35*, 2117−2121.
(65) Hlavenka, P.; Otto, R.; Trippel, S.; Mikosch, J.; Weidemüller, M.; Wester, R. Absolute Photodetachment Cross Section Measurements of the O^- and OH^- Anion. *J. Chem. Phys.* **2009**, *130*, 061105.
(66) Mandl, A. Electron Photodetachment Cross Section of Negative Ion of Fluorine. *Phys. Rev. A: At., Mol., Opt. Phys.* **1971**, *3*, 251−255.
(67) Swanson, J. R.; Armstrong, L. Multiconfiguration Hartree-Fock Calculation of Photoionization Cross-Sections of Rare-Gases. *Phys. Rev. A: At., Mol., Opt. Phys.* **1977**, *15*, 661−667.
(68) Mucha, M.; Frigato, T.; Levering, L. M.; Allen, H. C.; Tobias, D. J.; Dang, L. X.; Jungwirth, P. Unified Molecular Picture of the Surfaces of Aqueous Acid, Base, and Salt Solutions. *J. Phys. Chem. B* **2005**, *109*, 7617−7623.
(69) Alloway, D. M.; Hofmann, M.; Smith, D. L.; Gruhn, N. E.; Graham, A. L.; Colorado, R.; Wysocki, V. H.; Lee, T. R.; Lee, P. A.; Armstrong, N. R. Interface Dipoles Arising from Self-Assembled Monolayers on Gold: UV-Photoemission Studies of Alkanethiols and Partially Fluorinated Alkanethiols. *J. Phys. Chem. B* **2003**, *107*, 11690−11699.
(70) Galib, M.; Baer, M. D.; Skinner, L. B.; Mundy, C. J.; Huthwelker, T.; Schenter, G. K.; Benmore, C. J.; Govind, N.; Fulton, J. L. Revisiting the Hydration Structure of Aqueous Na^+. *J. Chem. Phys.* **2017**, *146*, 084504.
(71) Fulton, J. L.; Schenter, G. K.; Baer, M. D.; Mundy, C. J.; Dang, L. X.; Balasubramanian, M. Probing the Hydration Structure of Polarizable Halides: A Multiedge XAFS and Molecular Dynamics Study of the Iodide Anion. *J. Phys. Chem. B* **2010**, *114*, 12926−12937.
(72) Zhu, S. B.; Robinson, G. W. Molecular-Dynamics Computer Simulation of an Aqueous NaCl Solution: Structure. *J. Chem. Phys.* **1992**, *97*, 4336−4348.
(73) Olivieri, G.; Parry, K. M.; Powell, C. J.; Tobias, D. J.; Brown, M. A. Quantitative Interpretation of Molecular Dynamics Simulations for X-Ray Photoelectron Spectroscopy of Aqueous Solutions. *J. Chem. Phys.* **2016**, *144*, 154704.

https://doi.org/10.1021/acs.jpcb.1c04765
J. Phys. Chem. B 2021, 125, 10514−10526